Results in Physics 18 (2020) 103282

Contents lists available at ScienceDirect

Results in Physics

journal homepage: www.elsevier.com/locate/rinp

Effect of BN dimers on the stability, electronic, and thermal properties of monolayer graphene

Nzar Rauf Abdullah[a,b,c,*], Danyal A. Abdalla[a], Taha Y. Ahmed[a], Sarbast W. Abdulqadr[a], Hunar Omar Rashid[a]

[a] Division of Computational Nanoscience, Physics Department, College of Science, University of Sulaimani, Sulaimani, 46001 Kurdistan Region, Iraq
[b] Computer Engineering Department, College of Engineering, Komar University of Science and Technology, Sulaimani, 46001 Kurdistan Region, Iraq
[c] Science Institute, University of Iceland, Dunhaga 3, IS-107 Reykjavik, Iceland

ARTICLE INFO

Keywords:
Energy harvesting
Thermal transport
Graphene
Density Functional Theory
Electronic structure

ABSTRACT

We theoretically investigate structural stability, electronic and thermal characteristic of boron and nitrogen codoped monolayer graphene using density functional theory and Boltzmann transport equation. Three types of BN dimers, ortho, meta, and para dimers, are identified at different concentration ratios of B and N atoms. Our DFT calculations suggest that the BN ortho dimers are structurally favorable configurations due to the lowest required formation energy. At low doping ratio, large bandgap for BN para dimer is predicted leading to high Seebeck coefficient and figure of merit. In addition, a large deviation in the Wiedemann–Franz ratio is also seen, and a maximum value of the Lorenz number is thus found. In contrast, at high doping ratio, high Seebeck coefficient and figure of merit are found for BN ortho dimer and a low Seebeck coefficient for BN para dimer is noticed. Furthermore, a small deviation in Lorenz number is found for high doping ratio where the distance between BN pair is large.

1. Introduction

The two-dimensional graphene with honeycomb structure has exceptional properties such as high electrical [1,2], optical [3], thermal conductivity [4–6], and a high pronounced strength [7]. It also has exhibit high crystal quality and anomalous properties such as high electron mobility [8] and it thus attracted the attention of researchers and scientists to make it a candidate in the next-generation electronic materials [9]. Although graphene has a high thermoelectric power factor, its overall figure of merit (ZT) value is very low due to extremely high thermal conductivity [10,11]. The relatively low Seebeck coefficients (S) of pure graphene (PG) leads it also not to be a good candidate for thermoelectric devices [12,13]. Therefore, the scientists seek to enhance Seebeck coefficient with a low thermal conductivity in order to obtain high figure of merit.

Several methods have been suggested to enhance S of graphene based on modification of its structure. One can use geometrical effect or quantum confinement by reducing the width of a graphene channel to 100 nm which changes the S by orders of magnitude [14]. S can also be increased by using electron filtering technique in graphene superlattice. In this technique, the average value of S is proportional to the integral of the distribution of S versus energy of electrons. The low energy electrons in the distribution curve are observed to reduce the average S as their contribution is negative. They have shown that with the electron energy filtering technique using multiple graphene superlattice heterostructures, the low energy electrons can be filtered out and the S can be increased [15,16]. Applying strain with the doping engineering process may increase S. It has been found that the local strain arises misalignment of Dirac cones of different graphene sections in the k-space, and the doping engineering results their displacement in energy. The conduction gap is thus found to be a few hundred meV and S is enhanced to 1.4 mV/K by combining these two effects [17,18]. Doping of graphene is displayed to be an effective method for significantly enhancing S. In this process, doping increase phonon scattering by increasing defects and thus reduces the thermal conductivity, while the electrical conductivity and S are increased by the Fermi level downshift [19]. The opening bandgap of graphene can be used as a powerful method to enhance thermoelectric properties. The opening bandgap can be done either by doping heteroatoms [20], chemical functionalization [21], depositing graphene on states and using electric field [22]. The most workable technique to control the physical characteristics is doping process. For graphene, the natural candidate by substitutional doping is either Nitrogen (N) [23], Boron (B) [24], or co-doping by N and B [25], due to their similar atomic size of these dopants with the

* Corresponding author.
E-mail addresses: nzar.r.abdullah@gmail.com, nzar.abdullah@univsul.edu.iq (N.R. Abdullah).

https://doi.org/10.1016/j.rinp.2020.103282
Received 2 May 2020; Accepted 29 July 2020
Available online 04 August 2020

carbon and altering the electronic properties significantly and small alteration in the carbon lattice [26,27]. D'Souza and Mukherjee have shown that upon substituting boron nitride in place of a carbon isomer of graphene, a twofold increase in the S occurred. A similar increase in the S for bilayer graphene under the influence of a small electric field ~ 0.3 eV has been observed in their calculations [28].

In this work, we have studied the electronic and the thermal properties such as Seebeck coefficient and figure of merit of pure, and BN-codoped graphene in which equal amount of N and B atoms with difference concentrations varying from 6.25% (BN-structure) to 18.75% ($(BN)_3$-structure) and choosing different doping sites for each concentration [29]. Therefore, three types of BN dimers, ortho, meta, and para dimers, are identified at different concentration ratios of B and N atoms [30]. The main idea here is to use these three BN dimers to find the most stable structure. In addition, we can also determine the most active structure in thermoelectric performance.

In Section 2 the structure of graphene nanosheet is briefly overviewed. In Section 3 the main achieved results are analyzed. In Section 4 the conclusion of the results is presented.

2. Model and computational techniques

We consider $4 \times 4 \times 1$ supercell of graphene nanosheet consisting of 32 carbon atoms with a lattice constant 9.867 Å. The vertical separation between two sheets of graphene, z-axis, has been fixed at 20 Å to avoid the inter-planar interactions. The crystalline and molecular structure visualization programs called XCrySDen and VESTA are used for visualization of our models [31,32]. Structure relaxation and electronic calculations have performed by the plane-wave projector-augmented wave method implemented in the Quantum Espresso (QE) package [33]. The approach is based on an iterative solution of the Kohn–Sham equation of the density functional theory (DFT) by calculating self-consistently (SCF) a set of one-electron equations with the k-mesh grid $12 \times 12 \times 1$ [34,35]. For geometry optimizations, all the internal coordinates are relaxed until the force convergence is less than 10^{-4} eV/Å.

The calculations are carried out using the exchange–correlation functions which are realized in the non-relativistic Perdew-Burke Emzerhof pseudo-potential (PBE) [36]. The plane-wave cutoff energy was set to be 816.341 eV [37]. The calculations of lattice constants and the atomic coordinates at different doping concentrations are made by the minimization of total energy. For the band structure calculations, partial occupancy for each wave-function is determined using the Gaussian smearing method with smearing of 0.01 eV. In addition, the density of state (DOS) calculations are utilized using $45 \times 45 \times 1$ of k-mesh point. During the calculation process of non-SCF the partial occupancies are treated using the tetrahedron methodology.

Furthermore, we have used BoltzTrap software for calculating the thermal characteristics of the system [38]. The Seebeck coefficient characterizes the thermoelectric sensitivity of the materials and defined as $S = -\Delta V/\Delta T$, where ΔV is the voltage difference generated between the two ends of the junction of the system when a temperature difference ΔT is established between them. Hence a high value of Seebeck is required in thermoelectrical materials.

In the BoltzTraP, the Seebeck coefficient is given by [39]

$$S = \frac{ek_B}{N\Omega}\sigma^{-1}\int d\varepsilon\left(-\frac{\partial f_0}{\partial \varepsilon}\right)\left(\frac{\varepsilon-\mu}{k_B T}\right)\gamma_{n,\kappa}, \tag{1}$$

where

$$\gamma_{n,\kappa} = \sum_{n,\kappa} \tau_{n,\kappa}\,\vec{v}_{n,\kappa}\,\vec{v}_{n,\kappa}\,\delta(\varepsilon - \varepsilon_{n,\kappa}). \tag{2}$$

Herein, e refers to the unit charge, k_B is the Boltzmann's constant, N displays the number of k-points, Ω indicates the unit cell volume, σ is the electrical conductivity, ε represents the band energy, f_0 gives Fermi–Dirac distribution function, μ is the chemical potential, T stands for the temperature measured in Kelvin, τ refers to the relaxation time, v demonstrates the group velocity of the charges, and δ is the Dirac delta function. The subscripts κ and n mean the crystal momentum and the band index [38,40].

In addition, the dimensionless thermoelectric figure of merit introduces the efficiency of thermoelectric conversion is given by

$$ZT = \frac{S^2\sigma}{k_{th}}T. \tag{3}$$

Herein, $k_{th} = k_e + k_p$ is the sum of both electron and phonon thermal conductivity. We should mention that the thermometric properties are investigated at intermediate temperature range at 100 K in our work. In this range, the thermal conductivity of electrons will be dominated as it will be explained in the next section.

3. Results

In this section, we present the electronic and thermal properties of our model.

3.1. Pure graphene

First, we demonstrate the results of pure graphene as shown in Fig. 1, where the honeycomb structure of graphene (brown atoms) and electron charge distribution (a), band structure (b), Seebeck coefficient (c), the figure of merit (d), and Lorenz number (e) are plotted. The C–C bond length is found to be 1.42 Å which is in good agreement with the literature [41]. The electron charge density between the carbon atoms is high indicating a strong and stiffness of covalent bonds between the C atoms. Electronic band structure is calculated along the high-symmetry Γ-K-M-Γ directions. It obviously shows that the conduction and valence band are meeting at Fermi level or K point of the Brillouin zone, with DOS value very close to zero. As expected, very low S and ZT are found for the pure graphene which are 0.65 μV/K and 0.15 near Dirac point, respectively. In addition, a peak in Lorenz number at Fermi energy is found indicating a deviation in the Wiedemann–Franz law.

3.2. BN-codoped graphene

We now study the BN-codoped graphene and assuming three types of doping concentration ratios: First, one B (orange color) and one N (green color) atoms forming 6.25% of doping ratio are substitutionally doped in 32 host atoms which identifies as BN structure presented in Fig. 2(a–d). Second, two B and two N doped atoms consisting of 12.5% doping ratio shown in Fig. 3(a–d), where they are labeled as $(BN)_2$ structures. Third, three B and three N atoms with 18.75% doping ratio are considered as demonstrated in Fig. 4(a–d) that are defined as $(BN)_3$ structures.

For the above three doping concentration ratios, four BN dimers are assumed (a) B and N atoms are doped at ortho position (BN $_x$-1), in the dimer (b) same type of dopants (B or N) are placed at adjacent positions called meta position ($(BN)_x$-2), in the dimer (c) B and N are at para position ($(BN)_x$-3), and in the dimar (d) BN pair is at ortho position but the distance between two BN pairs is large ($(BN)_x$-4) [42].

The number of C–C, C–B, C–N, and B–N bonds in a monolayer nanosheet will affect the structural stability due to their bond energies. The bond energies can be arranged from the higher to lower energy as the following: B–N > C–C > N–C > B–C > B–B > N–N [43]. Consequently, a structure with high number of B–N bonds and less number of B–B and N–N bonds will be the most stable structure. To confirm the structural stability of our nanosheets we present Table 1 that shows the formation energy (FE), lattice constant (a), and bandgap of all nanosheets calculated via DFT. In the four BN-structures, the BN-1 is the most stable structure due to presence of B–N bond and less number of B–C and N–C comparing to other structures. Our DFT calculation also show that the formation energy of BN-1 structure presented in Table 1 is minimum indicating the most stable structure comparing to other BN

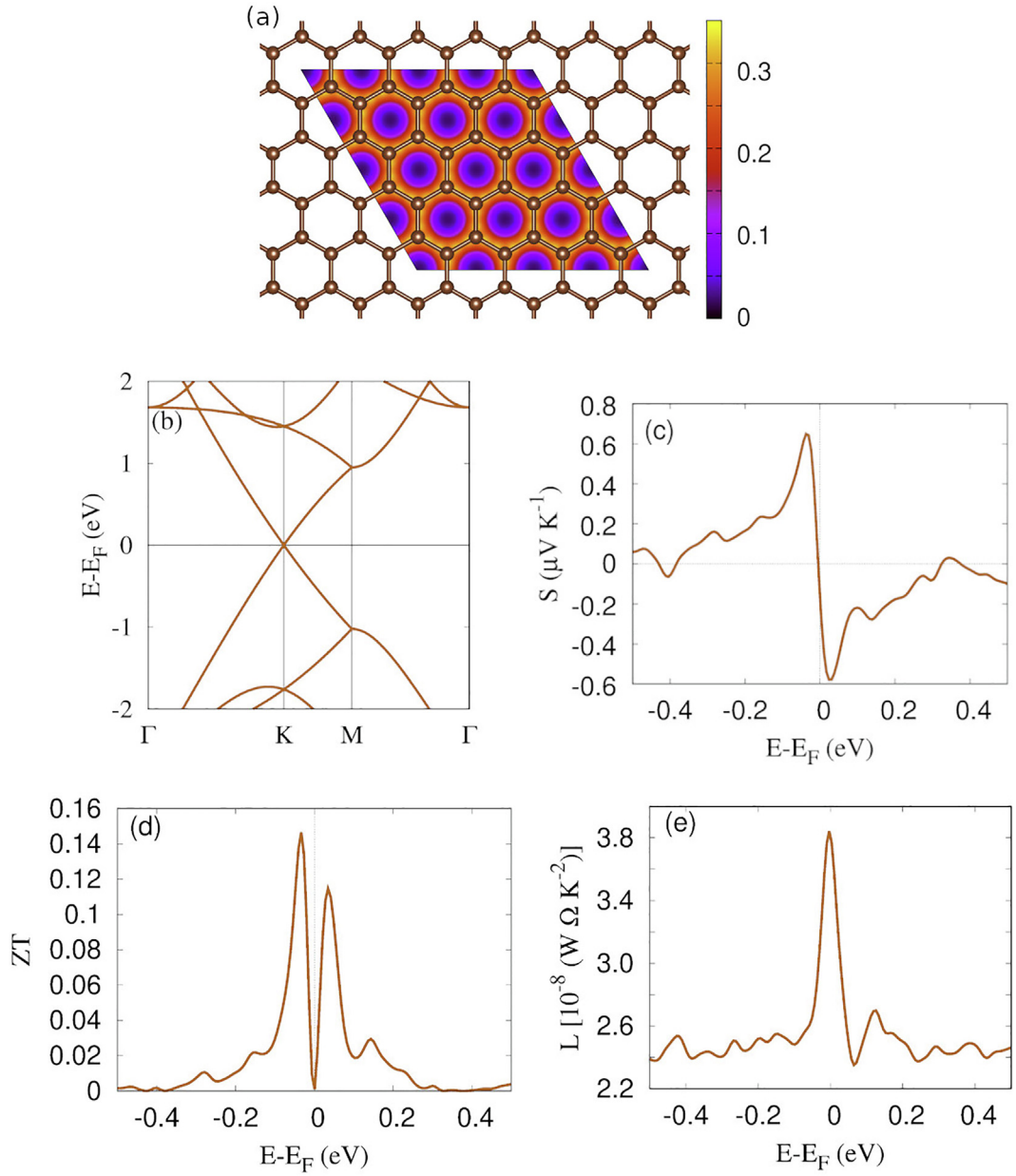

Fig. 1. (a) Pure graphene structure and electron charge distribution (contour plot), (b) band structure, (c) Seebeck coefficient, *S*, (d) the figure of merit, *ZT*, and (e) Lorenz number of pure graphene. The Fermi energy is set to zero.

structures [44]. Furthermore, the $(BN)_2$-1 and $(BN)_3$-1 nanosheets are also the most structural stable nanosheets because of their small formation energies and the B-N bonds are found in these nanosheets.

As a result, the aforementioned information and the formation energy given in Table 1 indicate that the BN ortho dimer is the most stable structure for all three of the doping ratios.

The B and N atoms substitutionally doped in graphene arises bond lengths modification between atoms, and several bonds can be found. The average bond length from long to short can be arranged as the following: B–B (1.53 Å) > C–B (1.49 Å) > B–N (1.45 Å) > N–N (1.44 Å) > C–C (1.42 Å) > C–N (1.40 Å). So, these change in bond lengths will cause distortion and thus break sublattice symmetry in BN codoped nanosheets. Consequently, it brings important modification in electronic characteristics at high concentration ratio [45].

But at low ratio of B and N atoms, 6.25%, such as the structures shown in Fig. 2(a–d), the bond modifications may not change much as a whole which makes almost the same size of those structures. This can be seen from the lattice constant shown in Table 1 where the lattice constant of all BN-structures is almost the same as of pure graphene. But we can still see different bandgap for BN-structures (see Fig. 2(e–h)). This can be explained by the aromaticity which introduces a charge delocalization. In BN-1, BN-3, and BN-4, an even number of π-bonds is found which indicates aromatic system because the B and N atoms are doped at the 1, 2 or 1, 4 positions of the hexagon indicating BN ortho or para dimers, respectively [46]. In addition, the BN-2 nanosheet is anti-aromatic structure with an odd-number of π-bonds since B and N atoms are located at positions 1 and 3 of the hexagon. Interestingly, band gap tuning has been attained for graphene systems with adsorbed higher aromatic molecules [47]. Therefore, the maximum bandgap is observed for the BN-4 structure.

Go back to the high concentration ratio of B and N atoms shown in Figs. 3 and 4. The structure with more number of long bonds (B–B bonds) will have a larger lattice constant (see Table 1). Typically, long bond lengths mean the electrons are less tightly bound to the atom, and

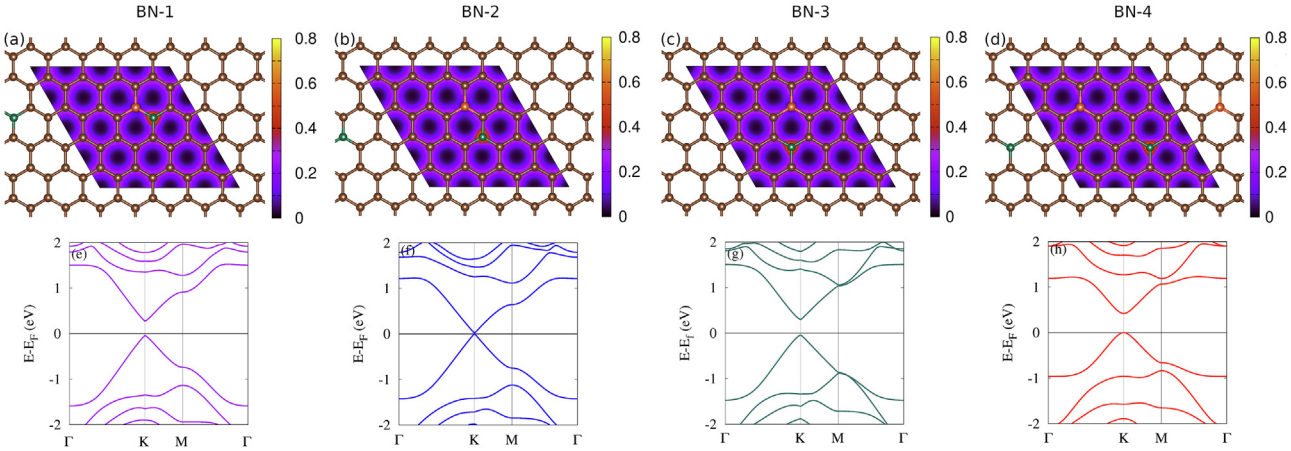

Fig. 2. The 4 × 4 × 1 supercell forming BN-1 (a), BN-2 (b), BN-3 (c), and BN-4 (d) structures with their electron charge distribution (contour plot) are plotted. The corresponding band structure of four structures are shown from (e) to (h). The Fermi energy is set to be zero.

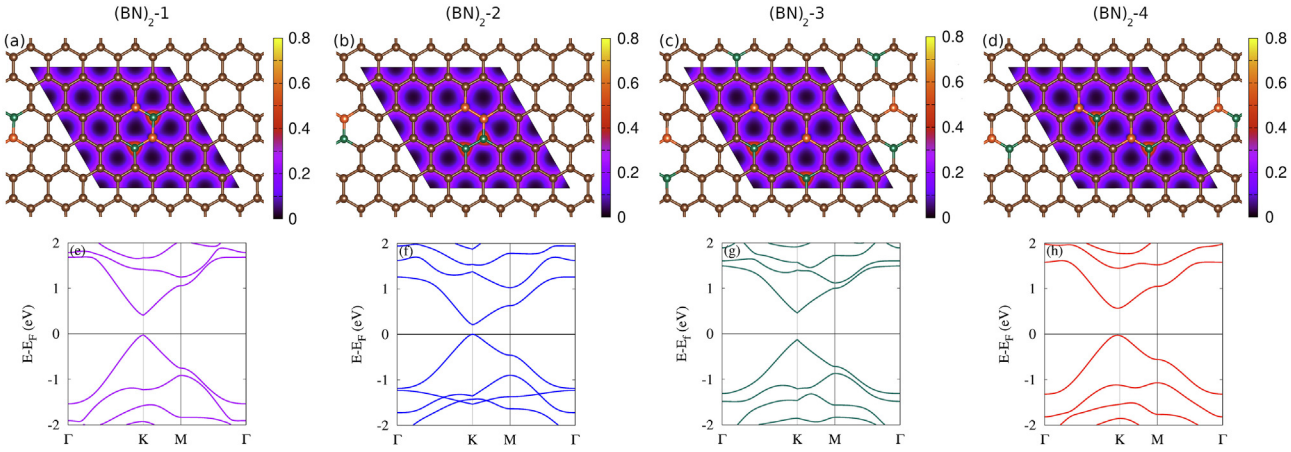

Fig. 3. The 4 × 4 × 1 supercell forming $(BN)_2$-1 (a), $(BN)_2$-2 (b)$(BN)_2$-3 (c), and $(BN)_2$-4 (d) structures with their electron charge distribution (contour plot) are plotted. The corresponding band structure of four structures are shown from (e) to (h). The Fermi energy is set to be zero.

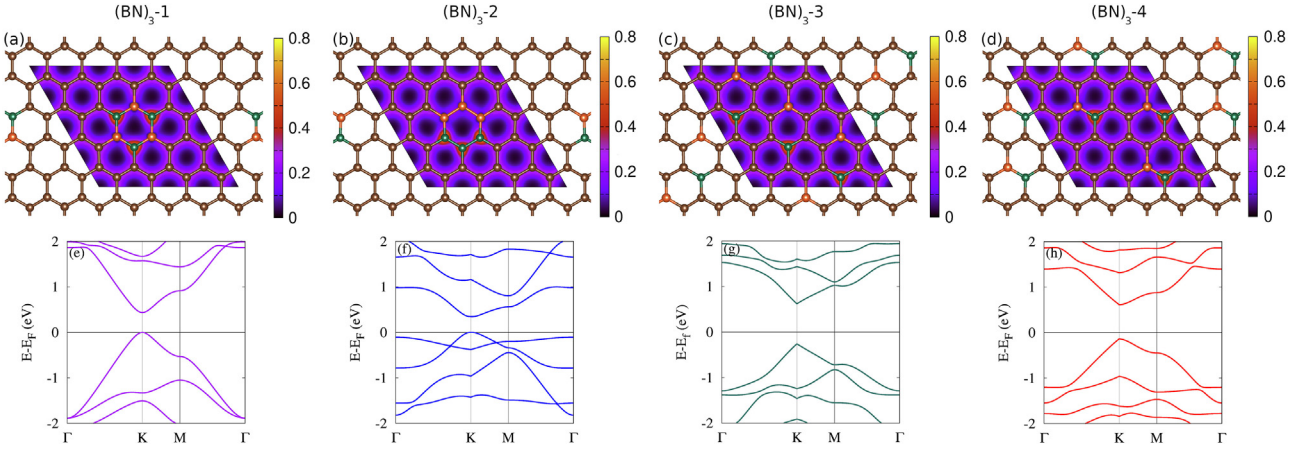

Fig. 4. The 4 × 4 × 1 supercell forming $(BN)_3$-1 (a), $(BN)_3$-2 (b), $(BN)_3$-3 (c), and $(BN)_3$-4 (d) structures with their electron charge distribution (contour plot) are plotted. The corresponding band structure of four structures are shown from (e) to (h). The Fermi energy is set to be zero.

hence require less energy to remove, leading to a decrease bandgap. Therefore, larger lattice constants correspond to lower bandgaps. Consequently, the minimum bandgap for $(BN)_2$-2 and $(BN)_3$-2 structures are found. So, we can say that in general, the longer the bond (nearest neighbor spacing), the longer the lattice constant and the smaller the band gap are obtained.

In addition, we found that a local depletion of the electron distribution around the B atom, and a local excess around the N atom, as presented in the contour plots of Figs. 2,3,4. These results are consistent with other calculations [26].

The thermal properties of the aforementioned structures are considered in this work. Thermal transport dependence on the electronic band structure has been verified experimentally [48]. We are interested in intermediate temperature, $T = 100$ K, where the electron and the

Table 1
Formation energy (FE), lattice constant (a), and bandgap of all BN-codoped structures.

Structure	FE (eV)	a (Å)	Bandgap (eV)
BN-1	−289.063	9.885	0.312
BN-2	−287.811	9.889	0.019
BN-3	−287.785	9.889	0.334
BN-4	−287.565	9.892	0.418
$(BN)_2$-1	−287.056	9.905	0.431
$(BN)_2$-2	−282.573	9.922	0.213
$(BN)_2$-3	−283.600	9.911	0.588
$(BN)_2$-4	−286.169	9.903	0.593
$(BN)_3$-1	−286.017	9.915	0.434
$(BN)_3$-2	−276.993	9.954	0.348
$(BN)_3$-3	−279.662	9.931	0.879
$(BN)_3$-4	−283.237	9.926	0.750

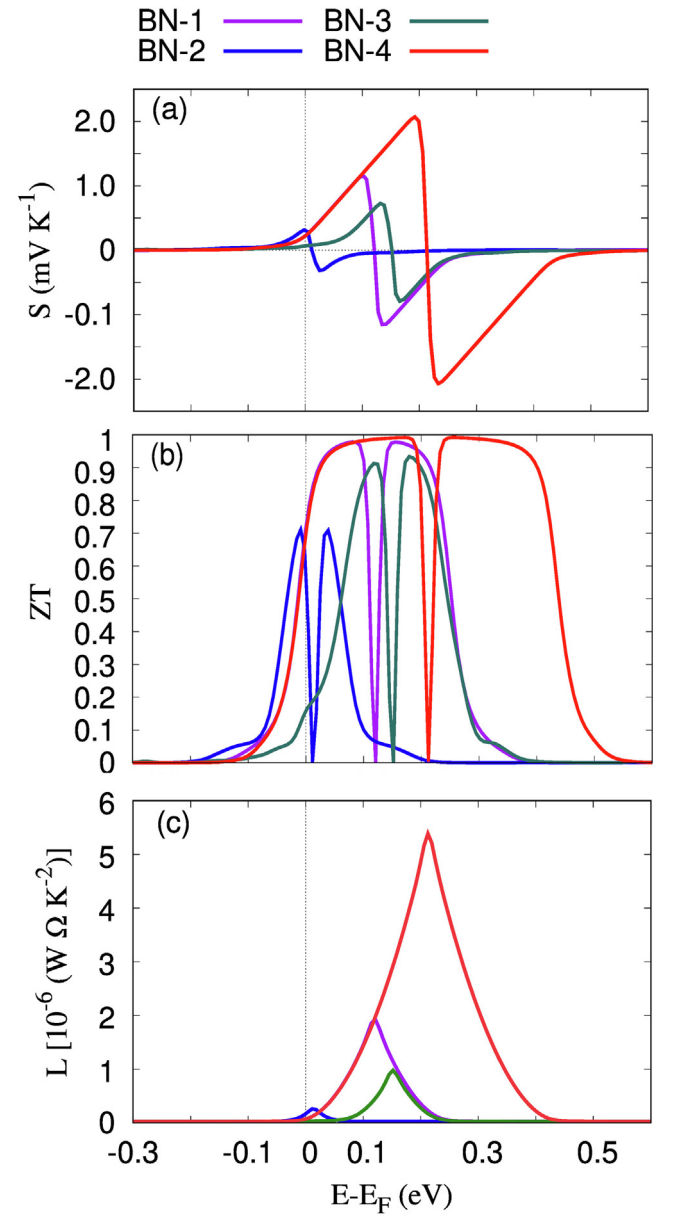

Fig. 5. Seebeck coefficient (a), figure of merit (b), and Lorenz number as a function of energy for BN-1 (purple), BN-2 (blue), BN-3 (green), and BN-4 (red) structures. The Fermi energy is set to be zero. (For interpretation of the references to colour in this figure legend, the reader is referred to the web version of this article.)

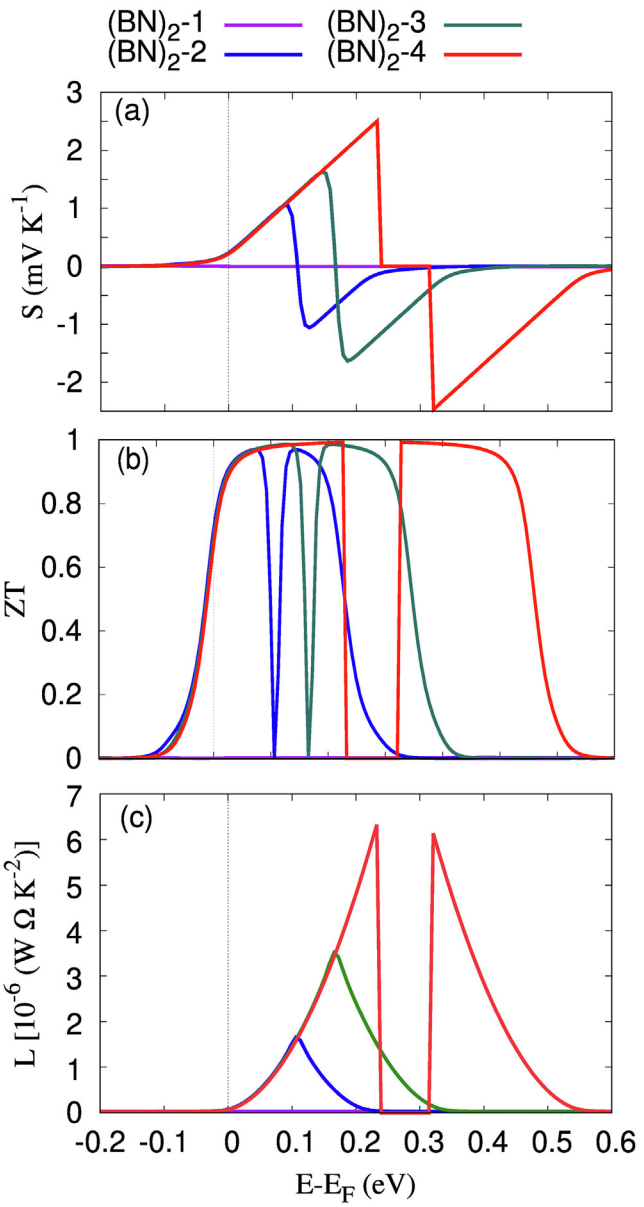

Fig. 6. Seebeck coefficient (a), figure of merit (b), and Lorenz number as a function of energy for $(BN)_2$-1 (purple), $(BN)_2$-2 (blue), $(BN)_2$-3 (green), and $(BN)_2$-4 (red) structures. The Fermi energy is set to be zero. (For interpretation of the references to colour in this figure legend, the reader is referred to the web version of this article.)

lattice temperatures are decoupled for low dimensional graphene structures [49,50]. At the intermediate temperature range, 10 − 160 K, the rate of energy transferred between the charge carriers and the acoustic phonons becomes very weak. We can thus use Boltzmann equation implemented in the Boltztrap to find transport coefficients of the electronic part of thermal properties. In Boltzmann theory, transport coefficients such as conductivity, Seebeck coefficient, and figure of merit depend on the band structure. Therefore, the bandgap plays an important role on electronic thermal characteristics.

In addition, the Wiedemann–Franz (WF) law for our model is assumed in which the ratio of electronic thermal conductivity, k_e, to electronic conductance, σ, can be defined as

$$L = \frac{k_e}{T\,\sigma} \tag{4}$$

which is constant for ordinary metals, where

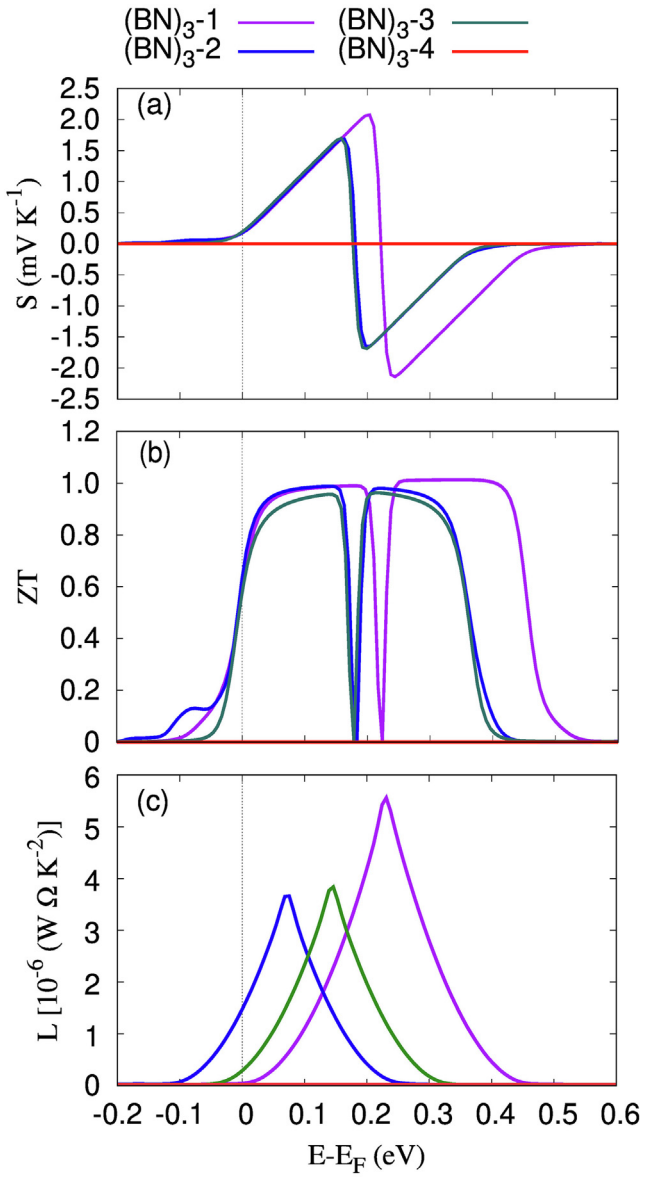

Fig. 7. Seebeck coefficient (a), figure of merit (b), and Lorenz number as a function of energy for $(BN)_3$-1 (purple), $(BN)_3$-2 (blue), $(BN)_3$-3 (green), and $(BN)_3$-4 (red) structures. The Fermi energy is set to be zero. (For interpretation of the references to colour in this figure legend, the reader is referred to the web version of this article.)

$L = L_0 = \pi^2 k_B^2/3e^2 = 2.44 \times 10^{-8}\,\mathrm{W\,\Omega\,K^{-2}}$, called the Lorenz number [51,52]. For graphene, the low chemical potential makes the Lorenz number sensitive to resonance scattering and the energy dependence of the relaxation time [53].

Fig. 5 indicates the Seebeck coefficient (a), figure of merit (b), and Lorenz number (c) of the BN-structures shown in Fig. 2 for BN-1 (purple), BN-2 (blue), BN-3 (green), and BN-4 (red) structures at 100 K.

In fact, semiconductors with low bandgaps effectively maximize free charge carrier contributions. The Seebeck coefficient is thus minimized since S is inversely proportional to charge carrier concentration [54]. Comparing to the thermal properties of pure graphene shown in Fig. 1, the Seebeck coefficient and figure of merit are maximized for BN-codoped structures due to opening the bandgaps. So, the maximum Seebeck coefficient for BN-4 structure, BN pair ortho dimer, (red color) is found due to the largest bandgap among the BN-structures. Consequently, the highest figure of merit is also observed for BN-4 and the maximum deviation in Lorenz number arises around the resonance state for BN-4.

The same scenario of thermal properties of BN-structure can be applied to $(BN)_2$-structure in which the maximum Seebeck coefficient and figure of merit are seen for $(BN)_2$-4 which has the maximum bandgap as they are presented in Fig. 6. A plateau in S and ZT around the Fermi energy may refer to the large bandgap. The maximum deviation in L also occurs for the $(BN)_2$-4.

In the high BN-codoping ratio, 18.75%, more B–B, N–N, and B–N bonds exist in BN-codoped structures leading to more distortion in the band structure as it was presented in Fig. 4. It arises the highest bandgap of $(BN)_3$-3 and $(BN)_3$-4 where the bandgap of $(BN)_3$-4 is further deformed. In this case, bottom of the conduction band is slightly shifted along the K-point which gives a small indirect bandgap (see Fig. 4h). This distortion in the band structures influences the thermal properties which is presented in Fig. 7. The Seebeck coefficient of the $(BN)_3$-1 with low direct bandgap is thus high comparing to large indirect bandgap of $(BN)_3$-4. The figure of merit becomes high and maximum deviation can also be seen for $(BN)_3$-1.

4. Conclusion

To summarize, we calculate the electronic and thermal properties of different BN dimers doped graphene nanosheets. Our results indicate that the meta BN dimers arise minimum bandgap due to presence of anti-aromatic structure and a low thermoelectric efficiency is thus seen. In contrast, the ortho and para BN dimers give rise to a large bandgap in which the bandgap of para BN dimer nanosheets is larger than that of ortho BN dimer structure at high B and N atoms of doping ratios. Consequently, the Seebeck coefficient and figure of merit are found to be high for para BN dimer nanosheets. But in the low doping ratio, the bandgap is found to be maximum for para BN pair nanosheet where the distance between BN pair is large leading to the enhancement of thermal efficiency. This can be seen as an optimizing way of bolometric applications of graphene based material devices.

Declaration of Competing Interest

The authors declare that they have no known competing financial interests or personal relationships that could have appeared to influence the work reported in this paper.

Acknowledgment

This work was financially supported by the University of Sulaimani and the Research center of Komar University of Science and Technology. The computations were performed on resources provided by the Division of Computational Nanoscience at the University of Sulaimani.

References

[1] Cusati T, Fiori G, Gahoi A, Passi V, Lemme MC, Fortunelli A, Iannaccone G. Electrical properties of graphene-metal contacts. Sci Rep 2017;7(1):5109. https://doi.org/10.1038/s41598-017-05069-7. URL:https://doi.org/10.1038/s41598-017-05069-7.

[2] Murata H, Nakajima Y, Saitoh N, Yoshizawa N, Suemasu T, Toko K. High-electrical-conductivity multilayer graphene formed by layer exchange with controlled thickness and interlayer. Sci Rep 2019;9(1):4068. https://doi.org/10.1038/s41598-019-40547-0. URL:https://doi.org/10.1038/s41598-019-40547-0.

[3] Narozhny BN. Optical conductivity in graphene: hydrodynamic regime. Phys Rev B 2019;100:115434 https://doi.org/10.1103/PhysRevB.100.115434. URL:https://link.aps.org/doi/10.1103/PhysRevB.100.115434.

[4] Li Q-Y, Xia K, Zhang J, Zhang Y, Li Q, Takahashi K, Zhang X. Measurement of specific heat and thermal conductivity of supported and suspended graphene by a comprehensive raman optothermal method. Nanoscale 2017;9:10784–93. https://doi.org/10.1039/C7NR01695F. URL:https://doi.org/10.1039/C7NR01695F.

[5] Fan Z, Pereira LFC, Hirvonen P, Ervasti MM, Elder KR, Donadio D, Ala-Nissila T, Harju A. Thermal conductivity decomposition in two-dimensional materials: application to graphene. Phys Rev B 2017;95:144309 https://doi.org/10.1103/PhysRevB.95.144309. URL:https://link.aps.org/doi/10.1103/PhysRevB.95.

144309.
[6] Sun Z, Yuan K, Chang Z, Zhang X, Qin G, Tang D. Efficient thermal conductivity modulation by manipulating interlayer interactions: A comparative study of bilayer graphene and graphite. J Appl Phys 126 (12):2019; 125104. arXiv:https://doi.org/10.1063/1.5115808, doi:10.1063/1.5115808. URL:https://doi.org/10.1063/1.5115808.
[7] Mazilova TI, Wanderka N, Sadanov EV, Mikhailovskij IM. Measurement of the ideal strength of graphene nanosheets. Low Temp Phys 44 (9):2018;925–929. arXiv:https://doi.org/10.1063/1.5052678, doi:10.1063/1.5052678. URL:https://doi.org/10.1063/1.5052678.
[8] Ullal CK, Shi J, Sundararaman R. Electron mobility in graphene without invoking the dirac equation. Am J Phys 87 (4):2019;291–295. arXiv:https://doi.org/10.1119/1.5092453, doi:10.1119/1.5092453. URL:https://doi.org/10.1119/1.5092453.
[9] Cao W, Jiang J, Xie X, Pal A, Chu JH, Kang J, Banerjee K. 2-d layered materials for next-generation electronics: opportunities and challenges. IEEE Trans Electron Devices 2018;65(10):4109–21.
[10] Anno Y, Imakita Y, Takei K, Akita S, Arie T. Enhancement of graphene thermoelectric performance through defect engineering. 2D Materials 2017;4(2):025019 https://doi.org/10.1088/2053-1583/aa57fc. URL:https://doi.org/10.1088.
[11] Abdullah NR, Marif RB, Rashid HO. Photon-mediated thermoelectric and heat currents through a resonant quantum wire-cavity system. Energies 2019;12(6). https://doi.org/10.3390/en12061082. URL:http://www.mdpi.com/1996-1073/12/6/1082.
[12] Dollfus P, Nguyen VH, Saint-Martin J. Thermoelectric effects in graphene nanostructures. J Phys Condens Matter 2015;27(13):133204 https://doi.org/10.1088/0953-8984/27/13/133204. URL:https://doi.org/10.1088%2F0953-8984%2F27%2F13%2F133204.
[13] Abdullah NR, Arnold T, Tang C-S, Manolescu A, Gudmundsson V. Photon-induced tunability of the thermospin current in a rashba ring. J Phys Condens Matter 2018;30(14):145303 https://doi.org/10.1088/1361-648x/aab255. URL:https://doi.org/10.1088%2F1361-648x%2Faab255.
[14] Harzheim A, Spiece J, Evangeli C, McCann E, Falko V, Sheng Y, Warner JH, Briggs GAD, Mol JA, Gehring P, Kolosov OV. Geometrically enhanced thermoelectric effects in graphene nanoconstrictions. Nano Lett 18 (12):2018;7719–7725, pMID: 30418781. arXiv:https://doi.org/10.1021/acs.nanolett.8b03406, doi:10.1021/acs.nanolett.8b03406. URL:https://doi.org/10.1021/acs.nanolett.8b03406.
[15] Mishra SK, Kumar A, Kaushik CP, Dikshit B. Enhancement of seebeck coefficient in graphene superlattices by electron filtering technique. Mater Res Express 2018;5(1):016301 https://doi.org/10.1088/2053-1591/aa9fd7. URL:ttps://doi.org/10.1088%2F2053-1591%2Faa9fd7.
[16] Gudmundsson V, Abdullah NR, Tang C-S, Manolescu A, Moldoveanu V. Cavity-photon-induced high-order transitions between ground states of quantum dots, Ann Phys 531 (11):2019;1900306. arXiv:https://onlinelibrary.wiley.com/doi/pdf/10.1002/andp.201900306, doi:10.1002/andp.201900306. URL:https://onlinelibrary.wiley.com/doi/abs/10.1002/andp.201900306.
[17] Nguyen MC, Nguyen VH, Nguyen H-V, Saint-Martin J, Dollfus P. Enhanced seebeck effect in graphene devices by strain and doping engineering. Phys E Low-dimensional Syst Nanostruct 2015;73:207–12. https://doi.org/10.1016/j.physe.2015.05.020. URL:http://www.sciencedirect.com/science/article/pii/S1386947715300552.
[18] Abdullah NR, Tang C-S, Manolescu A, Gudmundsson V. Manifestation of the purcell effect in current transport through a dot–cavity–qed system. Nanomaterials 2019;9(7):1023.
[19] Ma W, Liu Y, Yan S, Miao T, Shi S, Xu Z, Zhang X, Gao C. Chemically doped macroscopic graphene fibers with significantly enhanced thermoelectric properties. Nano Res 2018;11(2):741–50. https://doi.org/10.1007/s12274-017-1683-3. URL:https://doi.org/10.1007/s12274-017-1683-3.
[20] Hu C, Liu D, Xiao Y, Dai L. Functionalization of graphene materials by heteroatom-doping for energy conversion and storage. Prog Nat Sci Mater Int 2018;28(2):121–32. https://doi.org/10.1016/j.pnsc.2018.02.001. URL:http://www.sciencedirect.com/science/article/pii/S1002007118301175.
[21] Wang X, Li X, Zhang L, Yoon Y, Weber PK, Wang H, Guo J, Dai H. N-doping of graphene through electrothermal reactions with ammonia. Science (New York, N.Y.) 2009;324(5928):768–71. https://doi.org/10.1126/science.1170335. URL:https://doi.org/10.1126/science.1170335.
[22] Shemella P, Nayak SK. Electronic structure and band-gap modulation of graphene via substrate surface chemistry. Appl Phys Lett 2009;94(3):032101 .
[23] Tatarova E, Dias A, Henriques J, Abrashev M, Bundaleska N, Kovacevic E, et al. Towards large-scale in free-standing graphene and n-graphene sheets, Sci Rep 7 (1):2017;10175. doi:10.1038/s41598-017-10810-3. URL:https://doi.org/10.1038/s41598-017-10810-3.
[24] Xing M, Shen F, Qiu B, Zhang J. Highly-dispersed boron-doped graphene nanosheets loaded with tio2 nanoparticles for enhancing co2 photoreduction. Sci Rep 2014;4(1):6341. https://doi.org/10.1038/srep06341. URL:https://doi.org/10.1038/srep06341.
[25] Kim MS, Cho S, Joo SH, Lee J, Kwak SK, Kim MI, Lee J. N- and b-codoped graphene: a strong candidate to replace natural peroxidase in sensitive and selective bioassays. ACS Nano 2019;13(4):4312–21. https://doi.org/10.1021/acsnano.8b09519. URL:https://doi.org/10.1021/acsnano.8b09519.
[26] Wu M, Cao C, Jiang JZ. Light non-metallic atom (b, n, o and f)-doped graphene: a first-principles study. Nanotechnology 2010;21(50):505202 https://doi.org/10.1088/0957-4484/21/50/505202. URL:https://doi.org/10.1088%2F0957-4484%2F21%2F50%2F505202.
[27] Rani P, Jindal V. Designing band gap of graphene by b and n dopant atoms. RSC Adv 2013;3(3):802–12.
[28] D'Souza R, Mukherjee S. First-principles study of the electrical and lattice thermal transport in monolayer and bilayer graphene. Phys Rev B 2017;95:085435 https://doi.org/10.1103/PhysRevB.95.085435. URL:https://link.aps.org/doi/10.1103/PhysRevB.95.085435.
[29] Abdullah NR, Rashid HO, Kareem MT, Tang C-S, Manolescu A, Gudmundsson V. Effects of bonded and non-bonded b/n codoping of graphene on its stability, interaction energy, electronic structure, and power factor. Phys Lett A 2020;384(12):126350 https://doi.org/10.1016/j.physleta.2020.126350. URL:http://www.sciencedirect.com/science/article/pii/S0375960120301602.
[30] Abdullah NR, Rashid HO, Tang C-S, Manolescu A, Gudmundsson V. Modeling electronic, mechanical, optical and thermal properties of graphene-like bc6n materials: role of prominent bn-bonds, arXiv:2003.08467 [cond-mat.mes-hall] (2020). URL:https://arxiv.org/abs/2003.08467.
[31] Kokalj A. Xcrysden—a new program for displaying crystalline structures and electron densities. J Mol Graph Model 1999;17(3):176–9. https://doi.org/10.1016/S1093-3263(99)00028-5. URL:http://www.sciencedirect.com/science/article/pii/S1093326399000285.
[32] Momma K, Izumi F. Vesta 3 for three-dimensional visualization of crystal, volumetric and morphology data. J Appl Crystallogr 2011;44(6):1272–6.
[33] Giannozzi P, Baroni S, Bonini N, Calandra M, Car R, Cavazzoni C, Ceresoli D, Chiarotti GL, Cococcioni M, Dabo I, et al. Quantum espresso: a modular and open-source software project for quantum simulations of materials. J Phys Condens Matter 2009;21(39):395502 .
[34] Kohn W, Sham LJ. Self-consistent equations including exchange and correlation effects. Phys Rev 1965;140:A1133–8. https://doi.org/10.1103/PhysRev.140.A1133. URL:https://link.aps.org/doi/10.1103/PhysRev.140.A1133.
[35] Abdullah NR. Rabi-resonant and intraband transitions in a multilevel quantum dot system controlled by the cavity-photon reservoir and the electron-photon coupling. Results Phys 2019;15:102686 https://doi.org/10.1016/j.rinp.2019.102686. URL:http://www.sciencedirect.com/science/article/pii/S221137971932251X.
[36] Petersen M, Wagner F, Hufnagel L, Scheffler M, Blaha P, Schwarz K. Improving the efficiency of fp-lapw calculations. Comput Phys Commun 2000;126(3):294–309. URL:http://www.sciencedirect.com/science/article/pii/S0010465599004956.
[37] Perdew JP, Burke K, Ernzerhof M. Generalized gradient approximation made simple. Phys Rev Lett 1996;77:3865–8. https://doi.org/10.1103/PhysRevLett.77.3865. URL:https://link.aps.org/doi/10.1103/PhysRevLett.77.3865.
[38] Madsen GKH, Singh DJ. Boltztrap. a code for calculating band-structure dependent quantities. Comput Phys Commun 2006;175(1):67–71. URL:http://www.sciencedirect.com/science/article/pii/S0010465506001305.
[39] Oh MW, Wee DM, Park SD, Kim BS, Lee HW. Electronic structure and thermoelectric transport properties of agtlte: First-principles calculations. Phys Rev B 2008;77:165119 https://doi.org/10.1103/PhysRevB.77.165119. URL:https://link.aps.org/doi/10.1103/PhysRevB.77.165119.
[40] Abdullah NR, Tang C-S, Manolescu A, Gudmundsson V. The photocurrent generated by photon replica states of an off-resonantly coupled dot-cavity system. Sci Rep 2019;9(1):14703. https://doi.org/10.1038/s41598-019-51320-8. URL:https://doi.org/10.1038/s41598-019-51320-8.
[41] Avouris P. Graphene: Electronic and photonic properties and devices, Nano Lett 10 (11):2010;4285–4294, pMID: 20879723. arXiv:https://doi.org/10.1021/nl102824h, doi:10.1021/nl102824h. URL:https://doi.org/10.1021/nl102824h.
[42] Abdullah NR, Mohammed GA, Rashid HO, Gudmundsson V. Electronic, thermal, and optical properties of graphene like sic $_x$ structures: significant effects of si atom configurations, arXiv preprint arXiv:2004.01013 (2020).
[43] Bhandary S, Sanyal B. Graphene-boron nitride composite: a material with advanced functionalities, 2012.
[44] Rashid HO, Abdullah NR, Gudmundsson V. Silicon on a graphene nanosheet with triangle- and dot-shape: electronic structure, specific heat, and thermal conductivity from first-principle calculations. Results Phys 2019;15:102625 https://doi.org/10.1016/j.rinp.2019.102625. URL:http://www.sciencedirect.com/science/article/pii/S2211379719317140.
[45] Rani P, Jindal VK. Stability and electronic properties of isomers of b/n co-doped graphene. Appl Nanosci 2014;4(8):989–96. https://doi.org/10.1007/s13204-013-0280-3. URL:https://doi.org/10.1007/s13204-013-0280-3.
[46] Zhu J, Bhandary S, Sanyal B, Ottosson H. Interpolation of atomically thin hexagonal boron nitride and graphene: electronic structure and thermodynamic stability in terms of all-carbon conjugated paths and aromatic hexagons. J Phys Chem C 2011;115(20):10264–71. https://doi.org/10.1021/jp2016616. arXiv:https://doi.org/10.1021/jp2016616 URL:https://doi.org/10.1021/jp2016616.
[47] Chang C-H, Fan X, Li L-J, Kuo J-L. Band gap tuning of graphene by adsorption of aromatic molecules. J Phys Chem C 116 (25):2012;13788–13794. arXiv:https://doi.org/10.1021/jp302293p, doi:10.1021/jp302293p. URL:https://doi.org/10.1021/jp302293p.
[48] Wei P, Bao W, Pu Y, Lau CN, Shi J. Anomalous thermoelectric transport of dirac particles in graphene. Phys Rev Lett 2009;102:166808 https://doi.org/10.1103/PhysRevLett.102.166808. URL:https://link.aps.org/doi/10.1103/PhysRevLett.102.166808.
[49] Das Sarma S, Hwang EH. Density-dependent electrical conductivity in suspended graphene: approaching the dirac point in transport. Phys Rev B 2013;87:035415 https://doi.org/10.1103/PhysRevB.87.035415. URL:https://link.aps.org/doi/10.1103/PhysRevB.87.035415.
[50] Gabor NM, Song JCW, Ma Q, Nair NL, Taychatanapat T, Watanabe K, et al. Hot carrier–assisted intrinsic photoresponse in graphene. Science 334 (6056):2011;648–652. arXiv:https://science.sciencemag.org/content/334/6056/648.full.pdf, doi:10.1126/science.1211384. URL:https://science.sciencemag.org/content/334/6056/648.
[51] Saito K, Nakamura J, Natori A. Ballistic thermal conductance of a graphene sheet.

Phys Rev B 2007;76:115409 https://doi.org/10.1103/PhysRevB.76.115409. URL:https://link.aps.org/doi/10.1103/PhysRevB.76.115409.
[52] Sharapov SG, Gusynin VP, Beck H. Transport properties in the d-density-wave state in an external magnetic field: the Wiedemann-Franz law. Phys Rev B 2003;67:144509 https://doi.org/10.1103/PhysRevB.67.144509. URL:https://link.aps.org/doi/10.1103/PhysRevB.67.144509.
[53] Inglot M, Dyrdał A, Dugaev VK, Barna J. Thermoelectric effect enhanced by resonant states in graphene. Phys Rev B 2015;91:115410 https://doi.org/10.1103/PhysRevB.91.115410. URL:https://link.aps.org/doi/10.1103/PhysRevB.91.115410.
[54] Zou H, Rowe D, Min G. Growth of p- and n-type bismuth telluride thin films by co-evaporation. J f Cryst Growth 2001;222(1):82–7. https://doi.org/10.1016/S0022-0248(00)00922-2. URL:http://www.sciencedirect.com/science/article/pii/S0022024800009222.